J. Membrane Biol. 192, 45–63 (2003)
DOI: 10.1007/s00232-002-1063-z

The Journal of
Membrane
Biology

Gating Models of the Anomalous Mole-Fraction Effect of Single-Channel Current in *Chara*

U.P. Hansen, O. Cakan, M. Abshagen-Keunecke, A. Farokhi
Center of Biochemistry and Molecular Biology, Kiel University, Leibnizstr. 11, 24098 Kiel, Germany

Received: 28 May 2002/Revised: 25 September 2002

Abstract. The dependence of single-channel current on the Tl^+/K^+ mole fraction exhibiting a minimum at $[Tl^+]/[K^+]$ of about 1:15 is proportional to open probability in bursts. Five models are suggested to explain modulation of gating by the Tl^+/K^+ ratio. Three models start from a channel with 4 identical subunits, each with an allosteric binding site for K^+ or Tl^+. In the first model, ion binding is directly observable as a transition from one Markov state to another. This model can explain the dependence of the apparent single-channel current on Tl^+ concentrations. However, the predicted linear dependence on ion concentrations of the apparent rate constants was not observed in measurements in 25 or 250 mM KNO_3 and 250 mM Tl NO_3. The second model can overcome this problem by introducing saturation kinetics for ion binding. In the third model, gating is caused by inherent vibrations of the protein, and the rate constants of the related transitions depend on the occupation of the allosteric sites. The fourth model is based on the foot-in-the-door approach with the essential feature that two K^+ ions in the selectivity filter are necessary to keep the pore radius suitable for K^+ ions. The fifth model is also a foot-in-the-door model, but non-Markovian because, similar to model 3, it is assumed that the conformation of the protein (and thus the rate constants of the Markov model of the time series) depends on the force exerted by the temporal average over the states of a Markov model of ion occupation. These ions may reside in the pore itself or outside.

Key words: Allosteric sites—Conformational changes—Hidden Markov Models—K^+ channel—Selectivity filter

Introduction

Often, the current through a biological membrane in a mixture of certain ions is found to be smaller than in the pure solutions. This so-called anomalous mole fraction effect (AMFE) occurs in native plant membranes (K^+ channel in K^+/Tl^+: Tester, 1988; Draber, Schultze & Hansen, 1991; Farokhi, Keunecke & Hansen, 2000; Cl^- channel in Cl^-/SCN^-: Dietrich & Hedrich, 1998), in native animal membranes (K^+ channel in K^+/Tl^+: Hagiwara et al., 1977; Wagoner & Oxford, 1987; Lu et al., 2001; in K^+/Rb^+ or NH_4^+/Rb^+: Eisenman, Latorre & Miller, 1986; Ca^{2+} channel in Ca^{2+}/Ba^{2+}: Friel & Tsien, 1989; Hess & Tsien, 1984; Cl^- channel in Cl^-/SCN^-, Tabcharani et al., 1993), in Kv2.1/Kv1.3 chimeras (Kiss et al., 1998), or can be induced in the Shaker channel by mutations (Yool & Schwarz, 1996).

For many years, the AMFE was believed to be a stronghold of the Hille & Schwarz model (1978) with the essential feature of a multi-ion pore having two binding sites in the channel. The electrostatic repulsion force of a second ion is necessary to free the other ion from the binding site. This model was adopted by many workers (Ciani et al., 1978; Tester, 1988). In an alternative model, the Wu model (1991, 1992), the kinetic energy of the approaching second ion is necessary to free the first ion from a single binding site. Similar to the Hille-Schwarz model, the mutual liberation from the binding sites works best if the relevant parameters of both ions are equal, but in the Wu model the two binding sites are not necessary.

The suggested two binding sites of the Hille-Schwarz model got strong support from different findings. For instance, Baukrowitz and Yellen (1996) showed that the probability of an ion leaving the

Abbreviations: AMFE: anomalous mole fraction effect; C, G, Z: closed states; HMM: Hidden Markov model; O, A: open states; T, K, F: subunit of the channel binding Tl^+, K^+, or being empty, respectively.

Correspondence to: U.P. Hansen; email: uphansen@zbm.uni-kiel.de

channel decreased dramatically when no second ion was in the channel. It is tempting to assign two binding sites to those ones shown recently (Doyle et al., 1998; Morais-Chabral, Zhou & MacKinnon, 2001; Zhou et al., 2001) in the selectivity filter.

Both models assume that the AMFE is created by interaction of the permeating ions in a rigid channel structure. Recent results question the role of the multi-site channel for the creation of the AMFE. The findings of Baukrowitz and Yellen (1996) mentioned above can be explained by the findings of Zhou et al. (2001) that the pore collapses when the selectivity filter is depleted of K^+ ions. Further, the concept of strong binding sites in the K^+ channel has lost its physical fundament since Bernéche and Roux (2001) have revealed that the way through the pore is flat.

As an alternative, the concept of ion-induced modifications of channel structure came up with the suggestion of Pietrobon, Prod'hom & Hess (1988) that conformational changes of the dihydropyridine (DHP)-sensitive (L-type) Ca^{2+} channel induced by a permeating ion can be felt by a subsequent one. This was concluded from the observation of the destabilization of a protonated state of a group on the external channel surface by the permeating cation. Draber et al. (1991) suggested a lazy-state model (Hansen, Tittor & Gradmann, 1983) to explain the AMFE. In their investigations, a model of a channel that is activated by binding of K^+ to an allosteric site gave a better fit of the measured *I-V*-curves than the Hille-Schwarz model.

These findings led to the basic question that has to be answered before models can be created, namely, whether the AMFE is a gating or a permeation effect (Hansen, Keunecke & Blunck, 1997; Townsend & Horn, 1999). Farokhi et al. (2000) improved the temporal resolution of two-channel records in *Chara* so far that fast gating came into the accessible range of the direct fit of the time series with a Hidden-Markov model (Fredkin & Rice, 1992; Albertsen & Hansen, 1994; Klein, Timmer & Honerkamp, 1997; Sundermann & Zagotta 1999a,b; Zheng, Vankataramanan & Sigworth, 2001). It was found that the apparent reduction of single-channel current in a K^+/Tl^+ solution was identical to that obtained from averaging over a burst of fast gating. This showed that the AMFE in *Chara* can be explained by a gating effect. However, Farokhi et al. (2000) did not suggest a mechanistic model that could explain how a mixture of ions can influence gating in such a way that the apparent single-channel current is reduced. The construction of such an AMFE model has to deal with the influence of ions on gating properties and on selectivity. For both effects, many examples are reported by other workers.

The effect of ions on gating is involved in the shift in activation potential of the K^+ channel in guard cells with changes in external $[K^+]$ (Blatt, 1988) or in slowing down closing in squid giant axons (Swenson & Armstrong, 1981) or in chimeras of voltage-gated channels (Kiss & Korn, 1998). The effect of gating on outward K^+ current overrides that of driving force when external $[K^+]$ is increased (Wood & Korn, 2000) or when absence of external K^+ leads to conduction collapse (Pardo et al., 1992; Melishchuk, Loboda & Armstrong, 1998). Similar findings were also reported from the Na^+ channel (Townsend & Horn, 1999). However, Demo and Yellen (1992), similar to Levy and Deutsch (1996), found also speeding up of the opening rate with increasing $[K^+]_o$, indicating the variety of possible effects. Also an increase in chloride concentration is reported to enhance open probability of a chloride channel (Pusch et al., 1995; Pusch, 1996; Chen & Miller, 1996).

Draber and Hansen (1994) found that in the case of the voltage-dependent block of the K^+ channel in *Chara* by Cs^+ the rate constant of the transition into a closed state was proportional to Cs^+ concentration. The mutual relationship between ion binding and gating behavior became obvious in a Shaker channel with an engineered cysteine in the external P-loop. Binding of Zn^{2+} and Cd^{2+} drove the channel into the slow (C-type) inactivation state, but the state of the channel also exerted a strong influence on the K_d of Cd^{2+} binding, indicating conformational changes of the external mouth (Yellen et al., 1994). In the experiments of Perozo, Cortes & Cuello (1999), it was pH that changed the diameter of the inner gate.

The other effect required for an AMFE gating model is a parameter-induced change in selectivity. Changes in selectivity were found to be influenced by several factors (e.g., channel opening: Zheng & Sigworth, 1997; C-inactivation: Kiss et al., 1998, 1999; Larsson & Elinder, 2000; permeating ion: Kiss et al., 1998; Ogielska & Aldrich, 1999; Immke et al., 1999; ligand binding at an outer binding site: EF-hand of N-type Ca^{2+} channels, Feng et al., 2001). In most of these investigations, also a change in gating properties is reported. A change in gating properties upon ligand binding is well known at the cytosolic side (CNG channels: Ruiz & Karpen, 1999; Sundermann & Zagotta, 1999a,b; BK-channels: Moss & Magleby, 2001; Shi & Cui, 2001) or in glutamate receptors (Rosenmund, Stern-Bach & Stevens, 1998).

The locus of most of these modifications in selectivity and gating is assigned to the selectivity filter even though the site of interaction may be different. Ogielska and Aldrich (1999) suggested that a cuff of aromatic rings (W434 and W435) keeps the pore open by determining the location of Y445 (the middle of the conserved GYG motif of K^+ channels). During C-type inactivation this cuff relaxes and becomes too narrow for K^+ ions, but now Na^+ fits more snugly within the pore. Breaking of hydrogen bonds between E418 and V451 and V452 in Shaker is involved in the

changes of the diameter of this ring (Larsson & Elinder, 2000; Loots & Isacoff, 2000). However, the diameter of the selectivity filter can also be determined by its interaction with the main helices (Ogielska & Aldrich, 1999; Tabcharani et al., 1993).

The stimulus to base a gating model on these phenomena came from reports on the relationship between AMFE and C-inactivation (Kiss et al., 1998), or between AMFE and mutations influencing the structure of the P-loop (Tabcharani et al., 1993; Yool & Schwarz, 1996). The basic feature of the suggested model is the ion-dependent allosteric modulation of pore radius and thus of the selectivity of the K^+ channel. Assigning the observed gating phenomena of the AMFE to the selectivity filter is reasonable, as the rate constants observed by Farokhi et al. (2000) are very similar to those assigned by Zheng et al. (2001) to the selectivity filter. Five different models are considered for explaining the AMFE. Starting with simple models, the discussion of their failure to explain the temporal behavior leads to the scheme shown in Fig. 7 below.

1. Direct effect on gating of ion binding at an allosteric site: rate constants of binding = observed rate constants of gating.
2. Nonlinear effect on gating of ion binding at an allosteric site: gating is still caused by binding, but intermediate steps (ion binding and subsequent change of protein configuration) introduce saturation kinetics to the relationships between ion concentration and gating rate constants.
3. Modulation of gating by ion binding at an allosteric site: gating originates from temperature-induced vibrations, but the frequency of these vibrations is modulated by ion binding. This is similar to the findings of Ruiz and Karpen (1999) obtained from binding of cGMP to the four C-termini of the bovine retinal rod CNG channel.

The analysis started with model no. 1. Discrepancies between the predictions of the model and experimental results led to two refinements of the model (nos. 2 and 3). The improved models could explain the experimental findings, however, alternative models dealing with the effect of the permeant ions seem to be more likely in the light of recent results. Thus, two other models are suggested.

4. Occupation = gating. Similar to the Hille-Schwarz model, occupation with different ions blocks conduction, but not via insufficient balance of repulsion and binding of the permeating ions, but via conformational changes of the selectivity filter.
5. Modulation of gating. The average occupation of the pore determines the rate constants of inherent vibrations (transitions between Markov states) of the protein.

Material and Methods

Electrophysiological Measurements

Patch-clamp measurements were performed on cytosolic droplets of *Chara* as described previously by Farokhi et al. (2000). Briefly, cells of *Chara* were cut, and the cytosol formed droplets at the bottom of the experimental vessel in a solution of 250 mM KNO_3 (if not otherwise stated) and 5 mM $Ca(NO_3)_2$. NO_3^- rather than Cl^- was used in order to allow the replacement of K^+ by Tl^+. Sealing, however, seemed to work less well in NO_3^- than in Cl^-. According to Lühring (1986) and Sakano and Tazawa (1986), the membrane is a tonoplast.

The experimental setup is described in detail by Draber and Hansen (1994). Briefly, electrodes were made from borosilicate glass (Tl^+ experiments: Hilgenberg, Malsfeld, Germany) or quartz glass (25 mM K^+: Hereaus, Hanau, Germany) coated internally with Sigmacote (Sigma, Deisenhofen, Germany), drawn on an L/M-3P-A puller (List, Darmstadt, Germany) or a DMZ-Quartz-Puller (Zeitz, München, Germany), fire-polished, and filled with 250 mM KNO_3 + 5 mM $Ca(NO_3)_2$. External coating with Sylgard (Dow Corning, USA) was not employed. Instead, the technique of Keunecke (Farokhi et al., 2000) to keep the pipette with the excised patch (inside-out) close to the surface of the bathing solution (20 μM) reduced noise to $\sigma = 0.8$ pA at 50 kHz bandwidth. Bathing solution was equal to pipette solution. Patch-clamp current was recorded by a Dagan 3900A amplifier (Dagan, Minneapolis, Minnesota, USA) with a 4-pole anti-aliasing filter of 50 kHz. Data was stored on disk with a sampling rate of 200 kHz.

Definitions: Markov States, Single-Channel Currents, Gating and Permeation Effects

Modelling of ion channel behavior by Markov models has become a powerful and widely accepted tool (Ball & Rice, 1992; Korn & Horn, 1988; Yeo et al., 1988). The basic assumption is that the channel resides in discrete states and can perform abrupt jumps from one state to another. Thus, the kinetic behavior of a channel can be described by a set of states characterized by their symbols (conductances) and their gating behavior (rate constants of the transitions to other states).

Measurements in the temporal range defined by anti-aliasing filters in the kHz range have not revealed any necessity to use approaches other than Markov models (Korn & Horn, 1988). However, if a temporal resolution in the range of 1 ns were available, then the current would be a series of statistically distributed peaks presenting the transitions of individual ions. These peaks may be in opposite directions, as the measured net current is always the sum of inward and outward currents (Hansen et al., 1981). Having this in mind, we need a new definition of what is called a "state" and of what is called "real single-channel current".

Definition

The channel resides in a state from time t_1 to t_E (dwell time $t_E - t_1$) if the distribution $f(\Delta t_n)$ of time intervals between two subsequent passages of ions ($\Delta t_n = t_{n+1} - t_n$, with $t_1 \le t_n < t_{n+1} \le t_E$) can be described by a stationary function.

In the case of long-lived states, stationary holds if for all intervals $[t_u, t_o]$ (with $t_1 \le t_u \le t_n < t_{n+1} \le t_o \le t_E$) the same asymptotic distribution function $f(\Delta t_n)$ is found. In the case of short dwell times (t_E-t_1) of a Markov state, this test cannot be applied because the number of samples is not high enough to reach the asymptotic distribution, i.e., to smooth out statistical scatter. Then we have to assume that ergodicity holds. In that case, ensemble averaging can

replace temporal averaging. From an ensemble of experiments, sections of time series are selected that are assumed to be in the same state. From these sections, the distribution function is generated by taking one value $f(\Delta t_n)$ from every section. If the resulting distribution function $f(\Delta t_n)$ is independent of the values of n $(1 < n < E)$ chosen in individual sections, then a stationary state exists, and all records of the ensemble belong to the same stationary state.

Definition

The real single-channel current is the average of current values between t_1 and t_E if a stationary state (as defined above) exists between t_1 and t_E.

In long-lived states, single-channel current can be obtained from averaging over all ion movements between t_1 and t_E. In short-lived states, ensemble averaging as described above has to be done.

Definition

Apparent single-channel current is the single-channel current measured in a real experimental setup. This implies that averaging is done by the anti-aliasing filter and/or by the jump dectector (Schultze & Draber, 1993). If the integration time of this averaging process is much less than $t_E - t_1$, then the apparent single-channel current is equal to the real single-channel current. If the integration time is longer, then it may include averaging over states with high and low (e.g., open-closed) conductances, and the apparent single-channel current is a weighted average of the involved real single-channel currents.

Definition

An agent exerts a permeation effect on apparent single-channel current if it influences the parameters of the stationary distribution function $f(\Delta t_n)$ related to one state.

In this case, the real single-channel current or the average time between the passage of two ions is modified.

Definition

An agent exerts a gating effect on apparent single-channel current if it leaves the distribution function of the involved states unchanged but influences the distribution function of dwell times $(t_E - t_1)$ of the channel in these states.

Remark

The distinction between gating and permeation effect may become difficult or impossible because of special experimental or theoretical reasons.

These experimental reasons arise from an insufficient temporal resolution. This problem has become smaller with time. In the case of the Cs^+ block of the K^+ channel in *Chara,* the involvement of the fast gating was shown in 1993 and 1994 (Klieber et al., 1993; Draber & Hansen, 1994). For the AMFE, the temporal resolution was reached 6 years later (Farokhi et al., 2000).

The theoretical limitation arises when the vibrations of the protein that cause the transition from one Markov state to another are in the time scale of several ion transitions. Then, the distinction of gating and permeation effects is no longer possible. However, in the case of the AMFE investigated here, a single-channel current of 16 pA is equivalent to an average distance of 10 ns between two subsequent ions, and the dwell times related to the fast transitions of the Markov states are longer than 10 μs (Farokhi et al., 2000 and *see* Results below). This factor of 1000 eliminates the need to consider this theoretical problem now.

Simulation of Surrogate Time Series

In order to verify the results of the kinetic analysis and to check predictions of gating models, time series had to be generated from assumed rate constants. As described in detail previously (Blunck et al., 1998; Caliebe, Rösler & Hansen, 2002; Riessner et al., 2002), a temporal sequence of sojourns in the states of the assumed Markov model was generated, and the real single-channel current assigned to the actual state was superimposed by white noise as defined by the selected signal-to-noise ratio (SNR). The resulting signal was fed into the same filter as used for filtering of the experimental data (program available at http://www.zbm.uni-kiel.de).

Data Analysis

The apparent single-channel current was determined by fitting amplitude histograms of the measured time series with a sum of Gaussians and/or by a fit-per-eye, i.e., by cursor-controlled adjusting of lines in the middle of the clouds of data points in the time series displayed on the computer screen (http://www.zbm.uni-kiel.de/software). Riessner et al. (2002) have shown that in very noisy data the fit-per-eye yields by far more reliable results than the evaluation of amplitude histograms, because the fit-by-eye excludes ambiguous data points. The fit-by-eye is as effective as a new automatic level detection algorithm, probably because the human brain and the silicon computer use similar algorithms (Riessner et al., 2002, http://www.zbm.uni-kiel.de/software/leveldet.html), i.e., searching for putative jump-free sections of minimum noise, ranking the quality of these sections and determining their mean values.

The kinetic behavior of 1- or 2-channel records can be evaluated by means of dwell-time analysis (Blunck et al., 1998) or by a direct fit of the time series (HMM fit, Fredkin & Rice, 1992; Albertsen & Hansen, 1994; Klein et al., 1997; Sundermann & Zagotta 1999a,b; Zheng et al., 2001). Farokhi et al. (2000) have shown that the dwell-time analysis fails at the high temporal resolution required to study the gating effect of the AMFE in *Chara*. The direct fit of the time series (HMM fit) also results in fast rate constants that are too small. However, this can be corrected by studies with surrogate data (*see* above) as follows: The rate constants obtained from the fit are used to generate surrogate (simulated) time series. These time series are subject to the same filtering and analysis as the real data. If the rate constants delivered by the fit of the surrogate data are the same as those from the real data, then they are assumed to be correct. If they are smaller than those from the real data, then the search for the correct values starts as follows: the fast rate constants are increased (e.g., by 20%) and a new simulation is started. This is repeated until rate constants are obtained that are equal to those from the first run on the experimental data. Then, the (higher) rate constants used for this simulation run are taken as the real rate constants.

The Selection of the Markov Model

Evaluation of measured time series by a direct fit of the time series (HMM fit) and generation of surrogate data has to be based on a Markov model. For the investigations here, the *A-O-G-C-G* model was selected (linear Markov model with two open states *A, O*, and three closed states *G, C, Z*). This model gave the best fits also in the dwell-time analysis in *Chara* done by Lühring (1999) with the program of Blunck et al. (1998). However, as shown by Farokhi et al. (2000) other models, too, would do the job required here.

Modelling has two levels of truth. At the lower level, a model should generate the same kinetic behavior as the real process. However, the model does not necessarily reflect the physical mechanism of this process. This approach works fine in billions of automatic control units in technical systems. In science, often the second level is desired, where the parameters of the model should have well-defined counterparts in the real system.

Unfortunately, the solution of the "inverse problem", i.e., the evaluation of a model from measured data (Jackson, 1997), yields only the first level of truth. This results from the fact that many different Markov models create the same kinetic behavior. The investigator finds that several models give a perfect fit of the measured data, but he does not know which of the models is the true one, he even does not know whether the second-level true one is in the group of the investigated ones.

In the case of the paper of Farokhi et al. (2000), the first level of truth was sufficient. This resulted from the following scenario: The channel generates a time series. This time series has an unknown real single-channel current and a kinetic behavior generated by an unknown (Hidden) Markov model. The question is whether the measured apparent single-channel current is equal or smaller than the real single-channel current. The procedure to solve this question is to generate a time series with a kinetic behavior that is equal to that of the experimental time series. This can be done with a model of level 1. Then it can be checked whether the apparent single-channel current obtained by the analysis is equal or smaller than the "real single-channel current" used in the simulations. Farokhi et al. (2000) tested five different Markov models. They found that all models revealed a reduction of the single-channel current at AMFE conditions (20 mM Tl^+, 230 mM K^+) of mostly 25% and no reduction in pure K^+ solution. The existence of at least five "successful models" showed that the real model (level 2) cannot be determined from the present data.

Experimental Results and Modelling

Further Evidence that the AMFE in *Chara* is a Gating Effect

Farokhi et al. (2000) showed that a gating process was the cause of the reduction of apparent single-channel current in a solution of 20 mM $TlNO_3$ plus 230 mM KNO_3 plus 5 mM $Ca(NO_3)_2$. In Fig. 1, additional experiments at intermediate mole fractions are shown. Empty circles present measured apparent single-channel currents. Filled squares demonstrate the effect of fast gating on single-channel currents. For this purpose, the time series of the measured data were subject to a direct fit of the time series on the basis of a linear Markov model with the states *A-O-G-C-Z* (*A* and *O* = open states, *G, C, Z* = closed states). The reasons for selecting this model are given above. The HMM fit (Albertsen & Hansen, 1994) resulted in rate constants similar to those shown by Farokhi et al. (2000) or in Table 3 below (they are not displayed here, because they are intermediate magnitudes of minor importance for the question of current reduction). From these rate constants, surrogate data were generated on the basis of an *A-O-G-C-Z* model as described above. In the simulations, real single-channel current I_{sim} was assumed to be

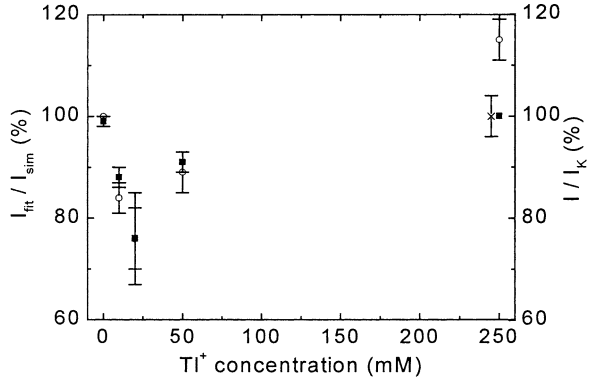

Fig. 1. Gating as the origin of the AMFE. Current reduction as determined by I_{fit}/I_{sim} (*filled squares*) was obtained from time series simulated on the basis of the *A-O-G-C-Z* Markov model with the rate constants obtained from an HHM fit of the measured time series. This is compared with the measured currents (*empty circles*). The deviation at 250 mM Tl^+ is not a wrong prediction, but results from the fact that the open-channel current of Tl^+ is higher. The cross gives the current that would have been measured if $I_{Tl} = I_K$. The data at $Tl^+/K^+ = 0$ and at the minimum of the AMFE are those of Farokhi et al. (2000). The other ones are from new experiments.

independent of the mole fraction and was set equal to the apparent single-channel current measured in pure K^+ ("pure" means "no Tl^+", but 5 mM Ca^{2+} were always included). Evaluation of the surrogate time series resulted in the reduced apparent single-channel currents I_{fit} presented by the filled squares in Fig. 1. In the presence of 20 mM Tl^+, a current reduction of $I_{fit}/I_{sim} = 25\%$ was observed, matching the experimental findings. In the case of pure K^+ and pure Tl^+, the reduction was not significant (1%). At intermediate concentrations, the reduction was smaller, and again the gating effect correctly predicts the measured values. The apparent deviation at 250 mM Tl^+ of measured i/i_K (Fig. 1) from the predicted I_{fit}/I_{sim} is not a failure of the theory, but results from the higher conductivity for Tl^+. If the current is scaled to I_K it coincides with $I_{fit}/I_{sim} = 1$ (*cross* in Fig. 1). The scatter bars for these "theoretical" data indicate that the generation of the surrogate data was done for each measured time series (three to four per data point).

The coincidence of the measured and simulated currents indicates that no other effect besides gating is required to create the measured mole fraction effect on single-channel current. Thus, Fig. 1 is a further confirmation of the statement of Farokhi et al. (2000) that the AMFE-induced reduction of apparent single-channel current in *Chara* is a gating effect as defined above.

Ligand Binding Causing Gating: General Features of the First Three Models

As mentioned in the introduction and in the discussion, modification of gating by ligand binding has

been described by many workers. In the first model it is tested whether this concept can be transferred to the AMFE in such a way that binding of ions to sites at the channel protein can cause the effects of the AMFE in *Chara*.

Actually, the K^+ channel in *Chara* has not yet been cloned; however, from its behavior it is assumed to be similar to the high-conductivity K(Ca) channel, another name for the BK channel (Tester, 1988). In the first three models, we assume that each of the four subunits has an allosteric binding site that can bind K^+ or Tl^+ with the rate constants $k_{1,1}$ and $t_{1,1}$, respectively, and release them with $k_{-1,s}$ and $t_{-1,s}$ respectively. Thus, binding of ions to each subunit can be described by a 3-state Markov model with the states K (K^+-bound), F (free), and T (Tl^+-bound). In a first approach, these four Markov models are independent, but cooperativity can easily be introduced by making the rate constants of ion binding and release dependent on the states of the other subunits.

The number of four is not crucial for the effects shown here, but it was used as a first approach because it was found in nearly all studies dealing with the effects of ligand binding, e.g., in the bovine cGMP-gated CNG channel or glutamate receptor mentioned above. When gating was slowed down by preoccupation with a high-affinity antagonist, the channel was found to pass through three distinguishable states with different conductances, and the number of four was verified by the finding that transition into the first state occurs with two time constants. The four-subunit model is not restricted to CNG channels. A similar relationship to the tetrameric structure emerged from studies of sublevels in delayed rectifier channels drk1 (Chapman, VanDongen & VanDongen, 1997) or in NMDA receptor channels (Schneggenburger & Ascher, 1997). Zheng et al. (2001) found staircase opening in the fine structure activation and deactivation of the Shaker channel and related the sublevels to the individual contributions of the four subunits. Allosteric binding of Mg^{2+} (or Ca^{2+}) to sites on each of the four subunits of the BK channel was described by Zhang, Solaro and Lingle (2001).

The macro-state of the channel is described by a four-letter symbol. KKKK means that all four binding sites are occupied by K^+: KKKT implies that three sites are occupied by K^+ and one by Tl^+, TTTT that all four sites are occupied by Tl^+, FFFF (F = free) is not occupied by any ion, KFKT binds two K^+, one Tl^+ and has one unoccupied binding site, etc.

Binding and release of an ion to or from an allosteric site in the four-subunit model is described by the equations

$$\frac{dK_b}{dt} = k_{1,1}KF - k_{-1,S}K_b \tag{1a}$$

and

$$\frac{dT_b}{dt} = t_{1,1}TF - t_{-1,S}T_b \tag{1b}$$

with K being the concentration of K^+, T the concentration of Tl^+, $k_{1,1}$ the rate constant of binding K^+, $k_{-1,S}$ that of releasing K^+, (suffix S indicates single subunit), $t_{1,1}$ the rate constant of binding Tl^+, $t_{-1,S}$ that of releasing Tl^+, K_b being the probability of the site having bound K^+, T_b being the probability of the site having bound Tl^+, F being the probability of the site being empty.

The sum of all states of the sites has to be 1. This automatically takes care of the normalization of the probabilities.

$$K_b + T_b + F = 1 \tag{2}$$

Model 1: Direct Effect of Ion Binding on Gating

Ion Binding and Apparent Single-Channel Current

The probabilites for occupation by K^+ are

$$p_K = K_b = \frac{\frac{k_{1,1}}{k_{-1,S}}K}{1 + \frac{k_{1,1}}{k_{-1,S}}K + \frac{t_{1,1}}{t_{-1,S}}T} \tag{3a}$$

by Tl^+

$$p_T = T_b = \frac{\frac{t_{1,1}}{t_{-1,S}}T}{1 + \frac{k_{1,1}}{k_{-1,S}}K + \frac{t_{1,1}}{t_{-1,S}}T} \tag{3b}$$

and of being unoccupied

$$p_F = F = \frac{1}{1 + \frac{k_{1,1}}{k_{-1,S}}K + \frac{t_{1,1}}{t_{-1,S}}T} \tag{3c}$$

Without cooperativity, the probability of being in a macro-state with κ sites being occupied by K^+, ϕ being free, 4-ϕ-κ being occupied by Tl^+ (κ, ϕ = 0, 1, 2, 3, 4) is

$$p^{(\kappa,\phi 4-\kappa-\phi)} = p^{\kappa}p^{4-\kappa-\phi}p^{\phi} \tag{4}$$

If the occurrence of the empty state F is rare ($k_{1,1}K > k_{-1,S}$ and $t_{1,1}T > t_{-1,S}$ then the "1" in the denominator of Eqs. 3a,b can be omitted and only the ratio between K^+ and Tl^+ binding becomes important

$$R = \frac{t_{1,1}k_{-1,S}}{t_{-1,S}k_{1,1}}\frac{T}{K}, \tag{5}$$

converting Eqs. 3a and 3b to

$$p_K = \frac{1}{1+R}; \quad p_T = \frac{R}{1+R}; \quad p_F = 0 \tag{6a, b, c}$$

Table 1. Rate constants and real open-channel current $I(\kappa,\phi,4\text{-}\kappa\text{-}\phi)$ used for the generation of the curves in Fig. 2

	$k_{1,1}$	$k_{-1,S}$	$t_{1,1}$	$t_{-1,S}$	$I_{(4K)}$ [pA]	$I_{(3KF)}$ [pA]	$I_{(3KT)}$ [pA]	$I_{(3TK)}$ [pA]	$I_{(3TF)}$ [pA]	$I_{(4T)}$ [pA]
1	40	250	400	250	4.0	4.0	4.0	5.5	5.5	5.5
2	40	250	400	250	4.47	0.0	4.47	5.5	0	5.5
3	40	250	400	250	4.47	0.0	2.7	3.3	0.0	5.5
4	40	250	600	250	4.47	0.0	4.47	0.0	0.0	5.5
5	40	250	400	250	4.47	0.0	4.47	1.0	0.0	5.5
6	40	250	400	250	4.47	0.0	0.6	0.6	0.0	5.5
7	40	250	400	250	4.0	4.0	0.0	0.0	5.5	5.5
8	40	250	400	250	4.47	0.0	2.7	0.0	0.0	5.5
9	40	250	400	250	4.47	0.0	0.0	0.0	0.0	5.5

States not mentioned in the Table have zero conductance. The rate constants $k_{1,1}$ and $t_{1,1}$ refer to 1 mM and have to be multiplied by the actual concentrations. Similarly, the real single-channel currents hold for 250 mM and thus have to be multiplied by a factor [ion]/250 mM.

The steady-state probabilities (Eq. 3) are used for calculating the apparent single-channel current. This implies that averaging over a burst of gated current is the basic mechanism causing the current reduction. This approach applies when the response time of the filter of the recording apparatus is longer than the dwell times in the open and closed states of the channel (Hansen et al., 1997). As mentioned above, this effect was very evident in the case of the Cs^+ block in *Chara* (Klieber & Gradmann, 1993), where the level detector could follow the gating at a sampling rate of 100 kHz, but could not at 5 kHz (Draber & Hansen, 1994).

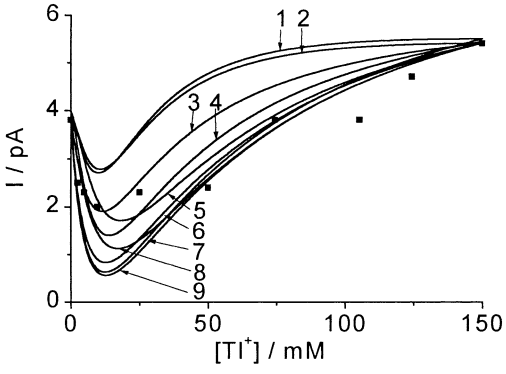

Fig. 2. Comparison of a measured AMFE curve (*squares*) in *Chara* (Hansen et al., 1997; Farokhi et al., 2000) with those predicted by model no. 1, showing the dependence of apparent single-channel current I (Eq. 7) on Tl^+/K^+ ratio ($[Tl^+] + [K^+] = 150$ mM) with the parameters shown in Table 1.

Generating the AMFE of the Apparent Single-Channel Current

If the time constants of the experimental setup are longer than those of the gating process, then the apparent (averaged) current at a given membrane potential can be calculated from the steady-state probabilities of the involved states

$$I = \sum_{k,\phi=0}^{k+\phi=4} p(\kappa,\phi,4-\kappa-\phi)\, I(\kappa,\phi,4-\kappa-\phi) \qquad (7)$$

with p being the occupation probability of the macrostate κK, ϕF, $(4\text{-}\kappa\text{-}\phi)T$ with the related real open-channel current $I(\kappa,\phi,4\text{-}\kappa\text{-}\phi)$.

It was tested whether a set of parameters can be found that results in a good fit of the experimental AMFE curve (apparent single-channel current *vs.* Tl^+ concentration in a solution of $[Tl^+] + [K^+] = 150$ mM as in Fig. 1) by Eq. 7. Nine different sets are given in Table 1 and the related curves (Eq. 7) are shown in Fig. 2 (smooth lines, squares present measured data points). The ratio of $t_{-1,1}/k_{1,1}$ in Table 1 determines the location of the minimum of the AMFE. It has to be mentioned that they have to be multiplied by the actual concentrations of the respective ion (Eq. 3). The magnitude of the backward reactions $t_{-1,S}$ and $k_{-1,S}$ determine the ratio of dwell times in the $4K$ (or $4T$) states and in the other states. Single-channel currents are zero for all states not shown in Table 1. The selection of the conducting states and the assignment of different real single-channel currents requires some comments.

Searching for some structural basis for our modelling, reports on changes of selectivity related to C-inactivation (e.g., Kiss & Korn, 1998; Ogielska & Aldrich, 1999) or the collapse of the pore structure in low K^+ solutions (Zhou et al., 2001) made us start with the hypothesis that the ion at the putative binding sites adjusts the pore diameter in such a way that the permeation of this ion is favored. This implies that $4K$ and $4T$ are conductive in all parameter sets. Curve no. *9* shows that restricting conductivity to $4K$ and $4T$ results in a minimum of the AMFE that is too low. Thus, also states with three equal ions (parameter set 1) were given non-zero real single-channel currents. Now, the minimum is not deep enough (Fig. 2), and if it is made deeper by choosing different values of the rate constants, then the dip moves too close to the K^+ side.

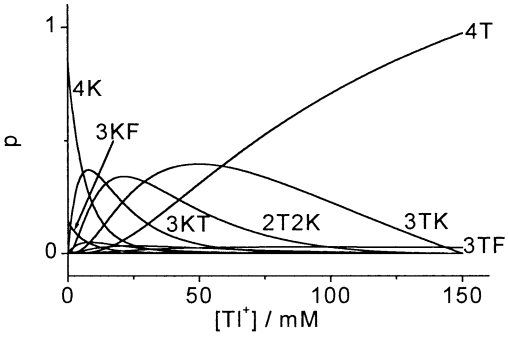

Fig. 3. Dependence of the probabilities of the states *KKKK*, *TTTT*, and the macro-states 3*KF*, 3*TF*, 2*K*2*T*, 3*KT*, 3*TK* on the Tl^+/K^+ ratio. Rate constants are those of curve *5* of Fig. 2.

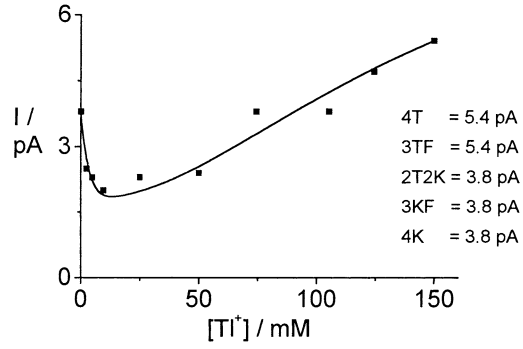

Fig. 4. Fitting the AMFE curve with a conducting state 2*K*2*T*. The data of the model were those of curve *8* in Fig. 2, but with a real open-channel current of 3.8 pA assigned not only to 4*K* and to 3*KF*, but also to 2*T*2*K* with $t_1 = 400$, $k_1 = 40$, and $t_{-1} = k_{-1} = 250$.

Transferring the observations of selectivity changes during C-inactivation to AMFE modelling, it may be assumed that the different states of the binding model have different real single-channel currents, because different binding states may cause different pore diameters and thus different conductances. Curves no. *3* and *5* come close to the experimental data. However, trying different data sets showed some basic problems of fitting the curves to the data. If the minimum is at the probably correct location (here at 10 mM Tl^+, because the data from Keunecke (Hansen et al., 1997; Farokhi et al., 2000) with $[K^+] + [Tl^+] = 150$ mM were taken as experimental data) then its current value is too low (curves no. *6* to *9*). On the other hand, if the current takes the correct value (curve no. *3*) at the minimum, then the current is too high in the range between the minimum and pure Tl^+: Curve no. *5*, which seems to come closest to all data points, has its minimum shifted to values of Tl^+ that are too high.

However, the problems are inherent to the model. The ratio R (Eq. 6) determines the minimum of the AMFE curve and saturation of Tl^+ occupation. High values of R (Eq. 5) move the region of the AMFE minimum to the left. But they also shift the saturation for Tl^+ occupation in Fig. 2 to the left. This leads to the bow of the curves above the data points on the right-hand side of the minimum. Even though there is some additional degree of freedom provided by the adjustment of the open-channel currents of 4*K*, 3*KT*, 3*TK*, 3*TF*, and 4*T*, the curve can be straightened only within narrow limits. A change in curve shape cannot be created by state 3*KF*, because the relationship between 4*K* and 3*KF* is highly constant in the range between $[Tl^+] = 0$ mM and the minimum of the AMFE curve (Fig. 3). Thus, the only free parameter is the sum of the currents assigned to these two states. Nevertheless, the ratio between 4*K* and 3*KF* becomes important when temporal behavior is considered because these states may be related to the measured states *A* and *O*, respectively.

The state 2*K*2*T* was not a favorite candidate under the starting assumption that binding adjusts the diameter of the pore for the binding ion. Nevertheless, the broad maximum of 2*K*2*T* in Fig. 3 made us test the assignment of non-zero single-channel current to 2*K*2*T*. Figure 4 shows that this results in a very good fit of the measured data. In Fig. 4, the open-channel current of 3*KT* is zero. This may be considered as a strange choice. However, 3*KT* prevents such a good fit as that one shown in Fig. 4, because a conducting state 3*KT* moves the minimum to the right-hand side. This can be compensated by stronger binding of Tl^+ (increasing the asymmetry factor R, Eq. 5). This stronger binding of Tl^+ leads to an earlier saturation of Tl^+ binding, and thus to a stronger upwards bow (as in the case of all curves in Fig. 2), which prevents a good fit at the right-hand side of the minimum. Plenty of further scenarios could be suggested and tested, e.g., assuming that there are two different classes of state 2*K*2*T* with K^+ being at neighboring sites or at opposite sites. However, this has not been extended because temporal behavior will reveal a more serious problem of model no. 1 that finally leads to a modification of this model.

Showing sets of parameters that result in successful fits (as in Figs. 2 and 4) is required for the next step testing the temporal behavior in order to get the following message at the end of the next paragraph: ''Even if your model succeeds in generating the correct AMFE curve (Fig. 4) you should not stop (as done in the past) because temporal behavior can falsify your model''.

Temporal Behavior: Different Number of States with and without Tl^+

Model no. 1 seems to be capable of modelling the AMFE. However, problems arise when gating be-

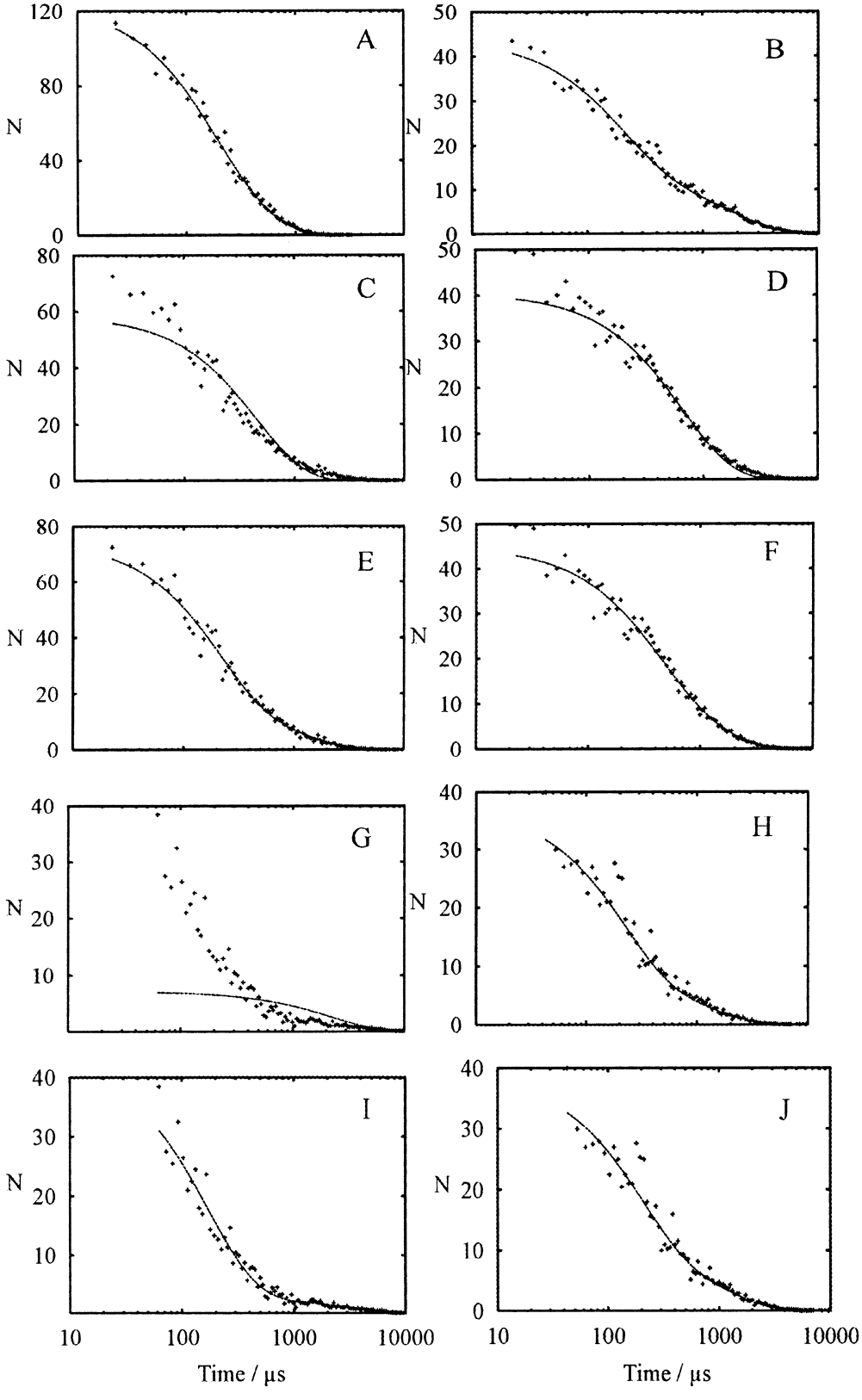

Fig. 5. Dwell-time histograms from simulated time series. Left-hand side (*A*, *C*, *E*, *G*, *I*): closed times. *Right-hand side* (*B*, *D*, *F*, *H*, *J*): open times. (*A*, *B*) The rate constants are those of curve *7* in Table 1 (or Fig. 2). (*A*, *B*) Model 1 in pure K^+ solution. (*C–J*) Model 1 in a solution of 230 mM K^+ and 20 mM Tl^+. Equal current of 4 pA was used for 4*K*, 3*KF*, 3*TF*, 4*T*. In (*C–F*) the current of 3*KT* was 3.8 pA and in (*G–J*) it was 0 pA. The simulated data were fitted with a three-state model (*A*, *B*, *C*, *D*, *G*, *H*) or with a four-state model (*E*, *F*, *I*, *J*). The dwell-time fit resulted in the rate constants shown in Table 2.

havior is inspected. For reasons arising from the investigations of Farokhi et al. (2000) and mentioned above in Materials and Methods, a simple linear 5-state model (*A-O-G-C-Z*) was employed for the HMM fit of the time series obtained from the K^+ channel in *Chara* with two open (*A, O*) and three closed states (*G, C, Z*).

In the case of measurements in pure K^+ solution, it is tempting to do the following assignment: $A = 4K$, $O = 3KF$, $G = 2K2F$, $C = K3F$, $Z = 4F$. However, in mixed solutions, it is questionable whether a 5-state model can present the four-segment model with $3^4 = 81$ states, even though they can be condensed to 15 classes of macro states, each comprising those states that are equivalent because of the 4-segment symmetry of the K^+ channel.

In order to find out how many states could be distinguished in a single-channel patch-clamp experiment if the K^+ channel in *Chara* would behave like model no. 1, simulated time series (surrogate data, *see* above) were generated for a 4-segment model on the basis of Eqs. 1a and 1b. In order to avoid the missed-events problem (Draber & Schultze, 1994), the rate constants were scaled down by a factor of 100 (and the results were scaled up by a factor of 100), and noise was not superimposed (this means that the results are an upper limit of what can be extracted from a real experiment). Under this condition, dwell-time analysis (Blunck et al., 1998) could be done instead of the time-consuming HMM analysis that is required for real data (Farokhi et al., 2000).

Figure 5 shows the results. The scatter results from the statistics of the Markov process. Figure 5 *A, B* verifies that the surrogate data in pure K^+ could be fitted by a three-state model *A-O-G*. A 5-state model (*not shown*) did not result in a better fit. This should not be taken as an objection against the *A-O-G-C-Z* model, as not all five kinetic states of the model of Farokhi et al. (2000) need to result from the same mechanism, and thus need not be generated by one model. Zheng et al. (2001) found that most closed states in Shaker K^+ channel are related to the main S6 (inner) gate, but some closed states are caused by the pore gate when the main gate is still open. Similarily, Proks et al. (2001) found independence of slow and fast gating and assigned burst kinetics to the selectivity filter. In Fig. 5, the burst kinetics are related to *A-O-G*, causing the flicker investigated here.

Four states are required for the fit of the surrogate data for 20 mM Tl^+ + 230 mM K^+ (minimum of the AMFE curve). The kinetic parameters are those of curve *7* in Fig. 2 but with equal open-channel current of the conducting states, which were $4K$, $3KF$, $3KT$, $3TK$, $3TF$, $4T$ for Figs. 5*C* to *F*. Figures 5*C*, *D* show that three states are not enough to fit the data, and a fourth state has to be introduced to fit the closed and open dwell-time histograms (Fig. 5*E, F*).

Table 2. Rate constants obtained from fitting of simulated data in Fig. 5.

Data set labels[1]	Rate constants
AB	$A \underset{21100}{\overset{20700}{\rightleftharpoons}} O \underset{36300}{\overset{14600}{\rightleftharpoons}} G$
EF	$A \underset{5200}{\overset{15800}{\rightleftharpoons}} O \underset{24600}{\overset{15200}{\rightleftharpoons}} G \underset{17400}{\overset{15800}{\rightleftharpoons}} C$
IJ	$A \underset{17100}{\overset{20600}{\rightleftharpoons}} O \underset{23500}{\overset{23900}{\rightleftharpoons}} G \underset{6800}{\overset{30000}{\rightleftharpoons}} C$
M	$A \underset{29900}{\overset{4800}{\rightleftharpoons}} O \underset{47100}{\overset{32500}{\rightleftharpoons}} G \underset{5200}{\overset{10200}{\rightleftharpoons}} C \underset{20}{\overset{260}{\rightleftharpoons}} Z$

[1]The labels correspond to the related pair of open- and closed-time histograms in Fig. 5. *M:* Averaged rate constants of Farokhi et al. (2000) measured in 250 mM K^+ at +80 mV. The rate constants of the bad fits (Fig. 5*C. D*, *G*, *H*) are not shown.

The question may come up whether this additional state results from the assignment of conductivity to $3KT$. Thus, simulations were done with $I(3KT) = I(3TK) = 0$. Again, the fit is bad for the three-state model and good for the four-state model. The good fit in Fig. 5*H* (which is better than in Fig. 5*D*) is obtained at the expense of the fit of the closed histogram in Fig. 5*G*. This is not unexpected as the additional state $3KF$ (and $3TK$) is assigned to the closed states.

The occurrence of the additional state in the presence of Tl^+ seems to be a contradiction to the experimental findings (Farokhi et al., 2000), even though it cannot be excluded that in *Chara* the new time constant was hidden because of coincidence with other time constants or because of limited resolution in noisy data. The rate constants obtained from successful fitting of the surrogate data are shown in Table 2. The obvious problem is that the relative magnitudes of the rate constants in Table 2 line *AB* do not correspond very well to measured ones in line *M*. However, it may be possible that a better correspondence can be achieved by introducing cooperativity factors making the rate constants dependent on the state of ion binding. This is not investigated here because other problems of the temporal behavior of model no. 1 are even more serious.

Temporal Behavior: Unpredicted Dependence of Rate Constants on Concentrations

Whereas the misfits of the rate constants of surrogate data and measured data are not so serious that they could not be overcome by some additional assumptions, new experiments shown in Table 3 provide more crucial objections against the simple model no. 1.

A basic feature of model no. 1 is the proportionality between rate constants and ion concentrations (Eqs. 3a to c). In order to test this, new

Table 3. Rate constants obtained from a direct HMM fit (Albertsen & Hansen, 1994) of new measurements at −100 mV in 25 mM K^+ and in 250 mM Tl^+ as compared with the rate constants at 250 mM K^+ and at the minimum of the AMFE (data from Farokhi et al., 2000, given without standard deviations)

Ion concentration	Rate constants
250 mM K^+	$A \underset{34500}{\overset{2500}{\rightleftharpoons}} O \underset{40200}{\overset{37900}{\rightleftharpoons}} G \underset{8900}{\overset{11400}{\rightleftharpoons}} C \underset{20}{\overset{960}{\rightleftharpoons}} Z$
25 mM K^+	$A \underset{8580\pm4900}{\overset{1100\pm700}{\rightleftharpoons}} O \underset{23200\pm4450}{\overset{25300\pm15000}{\rightleftharpoons}} G \underset{1710\pm970}{\overset{4420\pm2050}{\rightleftharpoons}} C \underset{110\pm90}{\overset{460\pm190}{\rightleftharpoons}} Z$
250 mM Tl^+	$A \underset{21060\pm120}{\overset{4040\pm340}{\rightleftharpoons}} O \underset{10850\pm2260}{\overset{19500\pm2260}{\rightleftharpoons}} G \underset{1160\pm330}{\overset{4844\pm1455}{\rightleftharpoons}} C \underset{21\pm1.5}{\overset{540\pm41}{\rightleftharpoons}} Z$
230 mM K + 20 mM Tl^+	$A \underset{1400}{\overset{2600}{\rightleftharpoons}} O \underset{28700}{\overset{56700}{\rightleftharpoons}} G \underset{4200}{\overset{7000}{\rightleftharpoons}} C \underset{60}{\overset{300}{\rightleftharpoons}} Z$

measurements were done in 25 mM KNO_3 (Table 3) and in 250 mM $TlNO_3$ in order to compare them with those in 250 mM K^+: The resulting time series were analyzed by a direct fit of the time series with a hidden Markov model (Fredkin & Rice, 1992; Albertsen & Hansen, 1994; Farokhi et al., 2000).

If we assign $A = 4K$ and $O = 3KF$ in the case of the measurements in pure K^+, and $A = 4T$ and $O = 3TF$ in pure Tl^+, then the following findings are expected:

1. The ratio k_{OA}/k_{AO} should be ten times lower in 25 mM K^+ than in 250 mM K^+.
2. The ratio k_{OA}/k_{AO} should be R times (Eq. 5, $R = 10$ in Table 1) higher in 250 mM Tl^+ than in 250 mM K^+.

These predictions are compared with the findings obtained in *Chara* in 250 mM Tl^+, 250 mM K^+ and 25 mM K^+ as shown in Table 3. In either case (comparing 250 mM Tl^+/250 mM K^+ or 250 mM K^+/25 mM K^+), there is no significant change in the k_{OA}/k_{AO} ratio. Even though the rate constants in 25 mM K^+ seem to be somewhat slower than in 250 mM K^+, the high scatter shows that this is not significant. More reliable than the absolute values of the rate constants is the ratio of forward to backward reaction. This is not changed by a factor of 10, as expected in either case (expected: 10-fold lower in 25 mM K^+ and 10-fold higher in 250 mM Tl^+, as compared to the data in 250 mM K^+). The high scatter of the absolute values of the rate constants obtained from the direct HMM fit of the time series may weaken this statement. However, the comparison with the data obtained in mixed solution (230 mM K^+ and 20 mM $T1^+$ presented in Table 3) shows that the analysis is capable of revealing a significant influence on the rate constants of the *A-O* transitions.

The results of Table 3 were unexpected as Lu et al. (2001) found a strong difference in gating kinetics of Kir2.1 in K^+ and Tl^+ solution, even with a decrease of time constants in Tl^+: However, these experiments were done on the ms scale (1 kHz filter), and the observed time constants correspond to the *C-Z* transitions of Table 3, which are not of interest in our studies, as these slow gating processes cannot contribute to the apparent reduction in single-channel current considered here (Fig. 1). If fast gating as observed in the *Chara* channel would occur also in Kir2.1, then the observed time constants in the ms range may be overestimated because interruption by fast gating would not be observed (Yeo et al., 1988; Colquhoun, Hawkes & Srodzinski, 1996). The magnitude of the rate constants of the *A-O-G* transitions in Table 3 corresponds to those of scheme I of Zheng et al. (2001) related to transitions in each of the four subunits on the outer pore gate, which also were revealed by an HMM fit of the time series.

Whereas the rate constants from the mixed solution led to a 25% reduction of current by the averaging property of the filter (Farokhi et al., 2000, Fig. 1), the reduction obtained from the rate constants in 25 mM K^+, 250 mM Tl^+ and in 250 mM K^+ resulted in a maximum reduction of 1%. All these findings together imply that the predicted changes in rate constants did not occur for 25 mM K^+ and 250 mM Tl^+ and indicate that model 1 in its simple form does not hold for the AMFE in *Chara*.

Model 2: Nonlinear Effect of Ion Binding on Gating

An attempt to overcome the failure of model no. 1 to predict the measured (in)dependence on concentrations of the ratio k_{OA}/k_{AO} is the introduction of saturation kinetics to the binding reactions. If the binding reactions are of the Michaelis-Menten-type, a half-saturation constant K_m of 1 mM may be reasonable because *Chara* lives in pond water. Then, both 250 mM and 25 mM would be far in the saturation region, and a change in the ratio k_{OA}/k_{AO} would not be expected in Table 3.

The introduction of saturation kinetics for K^+ or Tl^+ binding is provided by the introduction of an intermediate state in the binding reaction or in the release reaction (Eq. 8). It is assumed that this intermediate state I lies between the bound state B and the empty state E in the release reaction.

$$\begin{array}{ccc} B & \underset{k_{EB}}{\overset{k_{BE}}{\rightleftharpoons}} & E \\ & \searrow \quad \swarrow & \\ & I & \end{array} \tag{8}$$

If k_{BE} is very small, the backward reaction has to occur via I. Then, the following scenario holds for the backward reaction from B to E: When B has already lost its ion (B-I) and resides in I, the subunit is still not yet ready to bind an ion again. This needs an additional conformational change (I-E) in order to prepare the site for the binding of an ion. This scheme is similar to that in model 3. Thus, the other alternative is discussed here, i.e., assuming I in the straight path between E and B.

$$B \underset{k_{IB}}{\overset{k_{BI}}{\rightleftharpoons}} I \underset{k_{EI}\searrow}{\overset{\swarrow k_{IE}}{\rightleftharpoons}} E \tag{9}$$

means that after binding of the ion, the subunit needs some time to switch to the final configuration. The state F of the simple model 1 above is replaced by

$$F = I + E = \frac{k_{EI} + k_{IE}}{k_{EI}} I = r_1 I \tag{10}$$

with r_I being the reserve factor that merges all indistinguishable states into an apparent state (Hansen et al., 1983; Hansen, 1986).

This scheme would not lead to an extra time constant in the dwell-time histograms if the rate constants between E and I exceed the temporal resolution of the recording system. Such an assumption is feasible as binding of an ion (E-I) may be much faster than the subsequent change in the conformation of the protein (I-B). Such a situation is known from binding of cGMP that occurs with ca. 1 μs, but the measured Markov rate constants are at least 10 to 1000 μs. Thus, the recorded gating reflects the modulatory effect of binding (Sunderman & Zagotta, 1999a,b).

In the case of Eq. 10, the relative occupation probabilities of the states are obtained from the equations

$$B + I + E = 1 \tag{11}$$

and

$$B = \frac{k_{IB}}{k_{BI}} I, \quad E = \frac{k_{IE}}{k_{EI}} I \tag{12a, b}$$

Thus, the steady-state occupation probability of I is

$$I = \frac{1}{1 + \frac{k_{IB}}{k_{BI}} + \frac{k_{IE}}{k_{EI}}} = \frac{k_{BI} k_{EI}}{k_{EI} k_{IB} + k_{EI} k_{BI} + k_{IE} k_{BI}} \tag{13}$$

or in arrow presentation (Sanders and Hansen, 1981; Hansen 1986) in Eq 14.

$$B = \frac{\Rightarrow \rightarrow}{\begin{pmatrix} E & I & B \\ & \Rightarrow & \rightarrow \\ & \Rightarrow & \leftarrow \\ & \leftarrow & \leftarrow \end{pmatrix}} \quad I = \frac{\Rightarrow \leftarrow}{\begin{pmatrix} E & I & B \\ & \Rightarrow & \rightarrow \\ & \Rightarrow & \leftarrow \\ & \leftarrow & \leftarrow \end{pmatrix}}$$

$$E = \frac{\leftarrow \leftarrow}{\begin{pmatrix} E & I & B \\ & \Rightarrow & \rightarrow \\ & \Rightarrow & \leftarrow \\ & \leftarrow & \leftarrow \end{pmatrix}} \tag{14}$$

Each line gives the product of the rate constants presented by the arrows. The denominator is the sum of the lines. Source and sink state of the rate constants are identified by the letters at the base and the tip of the arrows. The double arrows denote the binding of K^+, k_{EI}. The equations for B and I have a Michaelis-Menten structure as indicated by the occurrence of the double arrow in the numerator and in some but not all lines of the denominator, resulting in

$$B = \frac{\text{const } [K]}{K_m + [K]} \tag{15}$$

implying that the increase with K^+ of the transitions into I and B is subject to saturation. This can explain that gating was not found to be significantly different in 250 and 25 mM K^+ (Table 3).

The statements of Figs. 2 and 3 can be transferred also to the model of Eq. 9 with the following replacements

$$k_1 = r_1 k_{IB}, \quad k_{-1} = k_{BI} \tag{16a, b}$$

with similar relationships for Tl^+ binding and release. The ratio t_I/k_I can be obtained from calculating the overall reactions K_{EB} for K^+ binding and $T1^+$ binding

$$\frac{t_1}{k_1} = \frac{t_{EI \cdot IB}/(t_{IE} + t_{IB})}{k_{EI \cdot IB}/(k_{IE} + k_{IB})} \cdot \frac{T}{K} \tag{17}$$

and thus it becomes obvious that the model of Eq. 9 leads to the same R as in Eq. 5, and thus to the same curves as in Figs. 2 and 4.

Such a model can cope with the above objections 1 and 2, namely that the occupation of $O = 3KF$ and

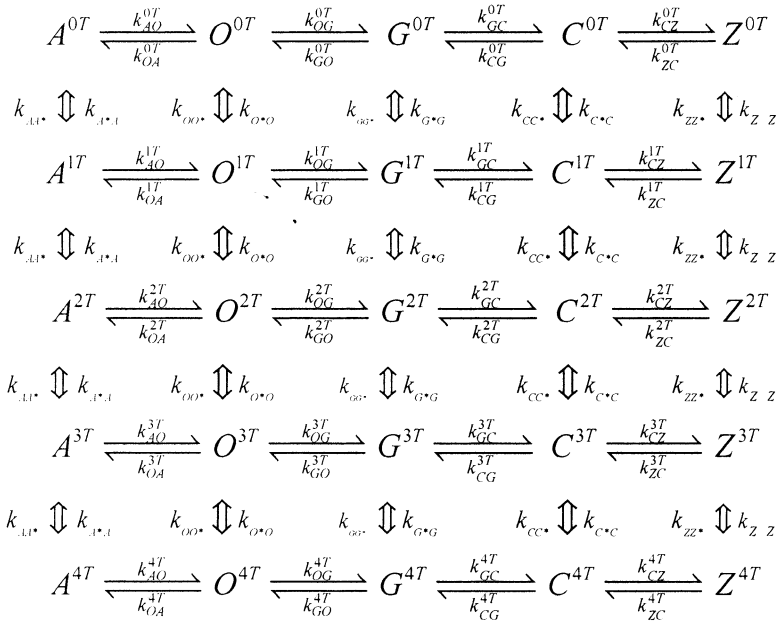

Fig. 6. Aggregated Markov Model consisting of five copies of the basic *A-O-G-C-Z* schemes each related to one of states (4-i)*KjT* of ion binding ($j = 0, 1,2,3,4$), which prevail under the condition that the empty binding state F is rare. $A^{0T} = A^{4K}$.

$A = 4K$ was not found to be directly related to the concentrations of the ions in single-channel experiments.

However, now a new problem arises. This behavior of the rate constants is not quite in line with the results of Farokhi et al. (2000). They found that the k_{AO}/k_{OA} ratio was changed under AMFE conditions, whereas the above model would leave the k_{AO}/k_{OA} ratio nearly constant. Instead, k_{OG} is influenced also, causing a decrease of the sum of A and O with $T1^+$ binding. The effect on k_{OG} is in line with the statement of Lu et al. (2001) that $T1^+$ dramatically destabilizes the open state of Kir2.1 channels. The problem of getting clear experimental decisions between an effect on k_{OA} or k_{OG} results from noise and high frequency of gating (25 to 50 kHz). Nevertheless, the next model can easily overcome the possible discrepancy between model prediction and experiment.

Model 3: Modulation of Gating by Ion Binding

If it is assumed that binding of an ion changes the rate constants of the inherent temperature-driven transitions of protein configurations (modulatory effect), then a Markov model is obtained that consists of multiple copies of the basic *A-O-G-C-Z* scheme with altered rate constants in each copy. In Fig. 6, the important part of this model is shown for the $jK(4-j)T$ ($j = 0, 1, 2, 3, 4$) aggregated Markov states, presenting the prevailing states under the condition that the empty state F is rare (Eq. 6). The structure of model 3 is similar to the general allosteric model of the CNG channel proposed by Ruiz and Karpen (1999) with the important message that cGMP binding does not introduce new Markov states, but modulates the rate constants of the transitions between open and closed. Also Moss and Magleby (2001) found that binding of Ca^{2+} to the Ca^{2+} bowl of BK channels does not introduce new kinetic states, but leads to a modulation of the rate constants. The BK channel is considered to be similar to the dominant *Chara* channel (Tester, 1988). The complexity of the model in Fig. 6 is much higher than that of model 1. However, as argued by Magleby (2001), sometimes complexity may lead to simplicity, especially when the complex model takes the structural properties of the protein into account.

In the case of pure solutions, the situation is quite simple. The rate constants obtained from the analysis of the measured time series are those of the reaction scheme ($A^{4K} = A^{0T}$)

$$A^{4K} \underset{k_{OA}^{4K}}{\overset{k_{AO}^{4K}}{\rightleftharpoons}} O^{4K} \underset{k_{GO}^{4K}}{\overset{k_{OG}^{4K}}{\rightleftharpoons}} G^{4K} \underset{k_{CG}^{4K}}{\overset{k_{GC}^{4K}}{\rightleftharpoons}} C^{4K} \underset{k_{ZC}^{4K}}{\overset{k_{CZ}^{4K}}{\rightleftharpoons}} Z^{4K} \tag{18}$$

and

$$A^{4T} \underset{k_{OA}^{4T}}{\overset{k_{AO}^{4T}}{\rightleftharpoons}} O^{4T} \underset{k_{GO}^{4T}}{\overset{k_{OG}^{4T}}{\rightleftharpoons}} G^{4T} \underset{k_{CG}^{4T}}{\overset{k_{GC}^{4T}}{\rightleftharpoons}} C^{4T} \underset{k_{ZC}^{4T}}{\overset{k_{CZ}^{4T}}{\rightleftharpoons}} Z^{4T} \tag{19}$$

respectively.

Figure 1 shows a linear dependence of gating on the $T1^+/K^+$ ratio in the range between 0 K^+ and minimum of the AMFE. The measurements of Farokhi et al. (2000) were single-channel measurements (even though two-channel records were evaluated). Thus, the model cannot account for this proportionality by ensemble averaging (mole fraction-de-

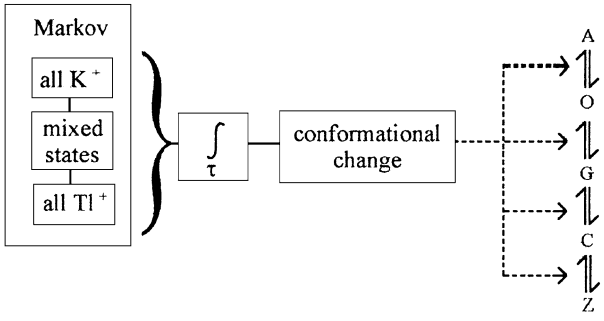

Fig. 7. Non-Markov model of gating. *Left-hand side*: Markov model of the occupation of allosteric binding sites (model 1) or of the sites inside the pore (Morais-Cabral et al., 2001). The average occupation of the Markov state influences via an integrating mechanism (time constant of conformational changes acting as a low-pass filter) the conformation of the channel protein. This conformation modulates the rate constants of the *A-O-G-C-Z* model of inherent channel gating.

pendent ratio of channels in $4K$, in $3KT$ and in other states) as in whole-cell recordings, but only by averaging in the time domain. This implies that binding and release at the allosteric sites has to be much faster than the transitions between states *A-O-G*.

If the Markov state presentation of Fig. 6 is taken seriously, then the apparent rate constants between A and O in mixed solutions (suffix a) with negligible occupation of $4T$ (Fig. 3 at 20 mM Tl^+) are

$$k^a_{AO} = \frac{k^{4K}_{AO}A^{4K} + k^{T}_{AO}A^{T} + k^{2T}_{AO}A^{2T} + k^{3T}_{AO}A^{3T}}{A^{4K} + A^{T} + A^{2T} + A^{3T}} \qquad (20)$$

$$k^a_{OA} = \frac{k^{4K}_{OA}O^{4K} + k^{T}_{OA}O^{T} + k^{2T}_{OA}O^{2T} + k^{3T}_{OA}O^{3T}}{O^{4K} + O^{T} + O^{2T} + O^{3T}} \qquad (21)$$

(states with more than $3T$ are neglected). The concentrations A^{4K}, A^T, A^{2T}, O^{4K}, O^T, O^{2T}, etc. are given by the above four-segment model (Fig. 3).

The numerical consequences of Eqs. 20 and 21 are probably in contradiction to the data of Farokhi et al. (2000). In some records, there is an up to 100-fold change in k_{AO} between the recordings at 250 mM K^+ and at the minimum of the AMFE curve. Probably this strong change in k_{AO} is not completely true, because the steady-state concentrations given by Farokhi et al. (2000) differ from the displayed rate constants, indicating the large scatter of the determinations. Nevertheless, if this factor were only about 10, this would have some consequences regarding Eqs. 20 and 21. The maximum decrease in the rate constants cannot be higher than the ratio A^{4K}/(all A) (in the case that the rate constants between states A and O with at least one Tl^+ bound are zero). Thus, A^{4K} has to decrease by at least a factor of 10 from the value in pure K^+ solution to the minimum of the AMFE curve. This is close to the behavior shown in Fig. 3, but some more numerical reserve would be desirable.

Thus, an alternative non-Markovian mechanism (non-Markovian in a sense that Markov fields are not constructed. They could create macrostates from states at different times) has to be considered. It is expected that binding and release at the putative binding sites have a much higher frequency than conformational changes of the protein. In that case, the protein senses an average force for conformational changes (Fig. 7). The resulting conformational change can influence the rate constants of the *A-O-G-C-Z* scheme without the numerical restrictions as given by Eqs. 20 and 21. However, this can no longer be described by one big Markov model. The model of Fig. 6 modified by Fig. 7 decouples gating events and ion binding, and thus it is capable of generating all the observed features:

- Independence of gating rate constants on K^+ concentration.
- No need to assume that the rate constants in pure K^+ and pure Tl^+ solutions reflect the ratio $k_{-1,S}\ t_{1,1}/k_{1,1}\ t_{-1,S}$.

Nevertheless, in spite of the success of the models in Figs. 6 and 7, two models based on the putative action of the ions in the pore are discussed because there are many hints in the literature that the foot-in-the door effect (Kiss et al., 1998; Lu et al., 2001) has to be taken into account.

Model 4: Foot-in-the-Door, Direct Action of Occupation

Farokhi et al. (2000) discussed whether a Hille-Schwarz (1978) model can create the gating that is responsible for the reduction of apparent single-channel current. They estimated that this model can explain the observed closed time, but would lead to open times that are by far too short because they are strongly related to the transfer rates of ions, which occur on a time scale 1000 times faster than the observed gating.

This objection against a crucial role of the ions in the pore can be overcome if we take into account that the ions in the pore control the diameter (Zhou et al., 2001, and all the literature mentioned in the Discussion). If we assume that the occupation of the pore by two K^+ ions adjusts the radius of the selectivity filter in such a way that the chance for Tl^+ to enter the filter is decreased by a factor of 1000 (and vice versa), then we get open times in the range of tens of μs, as observed by Farokhi et al. (2000). The open period is ended when a Tl^+ ion (due to the small but non-zero probability) enters the pore. Then the pore collapses and gets impermeable as two different ions are in the pore. The pore opens again when statistics bring the correct ion back into the pore. Such a model can also be described as a Markov model similar to model 1 (similar to the model of Morais-Chabral et al., 2001) and thus can easily generate the AMFE curves in

Figs. 1 and 2. The difference in the number of binding sites is not serious, especially as the actual number of relevant ions in the pore is unknown. It can also be four as in model 1 if we distinguish between the 2,4 and the 1,3 configurations, or if we include the cavity ion and the external one (Zhou et al., 2001). However, the experiments of Farokhi et al. (2000) and also the experiments related to Table 3 indicate that two open states are involved, which are not an inherent feature of this simple foot-in-the-door model.

Model 5: Foot-in-the-Door, Modulatory Effect of Occupation

Here, we consider an alternative mechanism starting from the finding of the *A-O-G-C-Z* analysis that the selectivity filter has two open states generated as follows: From the closed state *G*, the selectivity filter widens to the open state *O*. Then, the protein can make another conformational change into a state *A* that further stabilizes the open state. Model 5 is based on the assumption that the probability of the transition from state *O* into state *A* depends on the occupation of the pore. If the pore is occupied by two equal ions (K^+-K^+ or $T1^+$-$T1^+$) then the probability of entering state *A* is high. If the pore is occupied by different ions, then the rate constants get slower.

Kinetically, model 5 is very similar to model 3 (Fig. 7). As discussed above, the difference that we probably have two binding sites instead of four is not a serious objection against transferring the conclusions of model 3 to model 5. The more important difference to models 1 and 3 is that the access to the sites is not unrestricted, as the ions can only enter from the external or the internal side in single file.

The dependence on Tl^+/K^+ mole fraction is introduced according to the mechanism in Fig. 7: The vibration of the protein related to the transitions between *A*, *O* and *G* are slower (factor 1000) than the transfer times of the permeating ions. Thus, the movement of the protein is controlled by the average occurrence of K^+-K^+, K^+-Tl^+, or Tl^+-Tl^+ occupations of the pore. These occupations can be proportional to the $T1^+/K^+$ ratio as described by model 1. Again (Fig. 7), numerical restrictions like those of Eqs. 20 and 21 are not necessarily imposed as the relationships between protein vibration, average Tl^+/K^+ ratio in the pore and K^+/Tl^+ ratio in the solution is not expected to be linear.

Discussion

Gating as the Major Criterion for Falsifying AMFE Models

The inspection of temporal behavior forces modelling to move from model 1 (Fig. 2) to the non-Markov model of Fig. 7. Thus, the important message of modelling is the ion-dependent modulation of gating. The model of an inherently vibrating structure (Fig. 7, right-hand side) is a basic approach in the world of proteins and of great functional importance not restricted to channels. For instance, thermal fluctuations of the protein provide access for O_2 and CO_2 to the heme groups of myoglobin (Elber & Karplus, 1987). Thermal fluctuations are an important feature in the mechanism of the proton gradient-driven motion of the ATPase rotor (Junge, Lill & Engelbrecht, 1997). In Figs. 6 and 7, these fluctuations occur independently of the number of bound ligands, but the rate constants of the basic (Aggregated) Markov model are modulated by the time average of the number and species of bound ligands in the Markov model in Fig. 7, left-hand side.

Putative Structural Basis of Ion-dependent Gating

The model of the vibrating channel protein would also explain the finding of different selectivities in different channels. A nonspecific cation channel, as for instance the CNG channel involved in receptor-induced potentials (Balasubramanian, Lynch & Barry, 1997), would have a very wide amplitude of diameter oscillation, i.e., a very broad distribution of radii, thus giving ions of different kind a time to pass. A very selective channel should have a very rigid construction that results in a very narrow range of pore radii during an oscillation.

Candidates for the gates controlled by these oscillations are those suggested by Zheng et al. (2001): the (outer) pore gate, the (inner) S6 gate at the cytosolic side of the channel, and the N-type inactivation gate (chain and ball). Using chimeras of ROMK2 and IRK1, Choe, Sackin and Palmer (2000), too, found that effects of ion binding were related to an inner and an outer gate. The effect of Tl^+ seemed to be associated with both gates.

Preference for the pore gate comes from most studies dealing with the effects of ions on gating. Yool and Schwarz (1996) found that a mutation in the P-loop near GYG (T441S) caused a K^+/NH_4^+ AMFE in Shaker not found in wild type. This 3P-site (V121 in IRK1) played also an important role as modifying site in inward rectifiers (Choe et al., 2000). The role of the 3P position corresponds to the conclusion of Townsend and Horn (1999) that the activation gate of the Na^+ channel (as influenced by permeant cations) is on the cytoplasmic side of the selectivity filter, as supported by the finding that a pore residue (lysine 1418) is responsible for the activation of the Na^+ channel by permeant Na^+. The role of the selectivity filter is also favored by other authors (Matteson & Swenson, 1986; Demo & Yellen, 1992; Kiss, LoTurco & Korn, 1999; Proks et al., 2001).

Mutation of a binding site at the outer pore mouth (D378Y) of Kv2.1 influenced ion conduction and blockade (Kirsch, Pascual & Shieh, 1995). Similarly, one component of K^+-dependent potentiation of current in Kv2.1 and mutants was found to be related to the influence of two lysines at positions 356 and 382 in the outer vestibule (Wood & Korn, 2000). Yellen et al. (1994) demonstrated the role of the external mouth for Cd^{2+}- and Zn^{2+}- induced gating in a T449C Shaker mutant.

Time scale as an argument against the involvement of the outer gate may arise from the fact that normally the pore gate is associated with slow processes like C-type inactivation (Kiss et al., 1998, 1999; Larsson & Elinder, 2000), whereas the rate constants in the *A-O-G* subscheme of Farokhi et al. (2000) are in the range above 10 000 s^{-1}. However, the HMM analysis of intermediate gating steps in Shaker K^+ channels thought to be associated with the pore gate revealed rate constants in the same temporal range (Zheng et al., 2001). Sundermann & Zagotta (1999a,b) found rate constants in this range modulated by cyclic nucleotide binding on the cytosolic side of CNG channels, and brief life times in the range of tens of μs were found in BK channels (Ferguson, McManus & Magleby, 1993). Thus, rate constants do not provide a means of ruling out a special gate as the locus of fast gating events.

Hidden Rate Constants of Ion Binding

The integrating unit in Fig. 7 implies that ion binding in the left-hand Markov model is faster than the rearrangements of the protein acting on the gating model at the right-hand side. Thus, these putative very fast rate constants of ion binding do not become obvious in the measured rate constants of the transitions between the Markov states of the time series according to Figs. 6 and 7. This has already been reported for the bovine retinal rod CNG channel (Ruiz & Karpen, 1999) and for the effect of Ca^{2+} on the BK channel (Rothberg & Magleby, 2000). Only if ligand binding is slowed down artificially, it can be observed (Rosenmund et al., 1998). With respect to this, it is important that Moss and Magleby (2001) did not find a change in the number of kinetic states with Ca^{2+} binding, but a modulation of the rate constants.

The Physical Background of the Ion-binding Markov Model in Fig. 7

The difference between model 3 and model 5 is in the location of the Markov model of ion binding at the left-hand side of Fig. 7. Models 1 to 3 assume real allosteric binding sites somewhere at the protein. Models 4 and 5 deal with the mutual forces between selectivity filter and permeating ions. When introducing model 1, references dealing with ligand binding were given. However, nice examples for a tetrameric model like that in Fig. 2 have only been reported for the cytosolic side (Ruiz & Karpen, 1999; Sunderman & Zagotta 1999a,b; Moss & Magleby, 2001; Zhang, Solaro & Lingle, 2001). Reports on allosteric binding sites at the outer mouth are rare (EF-hand at the Ca^{2+} channel: Feng et al., 2001; sites for binding Cs^+ or Na^+ in the NMDA receptor: Antonov & Johnson, 1999; agonist binding sites on the glutamate receptor: Rosenmund et al., 1998). In Shaker, an engineered cystein provides binding of Cd^{2+} with an allosteric effect on gating (Yellen et al., 1994). The absence of reports on native allosteric binding sites on the outer P-loop (even though there are charged residues like E418 or E422 in Shaker [Larsson & Elinder, 2000] or K356 in Kv2.1 [Immke et al., 1999]) does not imply that there are no such bindings sites. Further, the allosteric sites need not be restricted to the immediate neighborhood of the selectivity filter, as also the S3-S4 linker was found to play a role in channel activation (Mathur, Zheng & Sigworth, 1997).

On the other hand, interaction between permeating ion and selectivity filter (foot-in-the-door model: Swenson & Armstrong, 1981; Demo & Yellen, 1992), is supported by a wide field of investigations already mentioned above (Kiss et al., 1998, 1999; Ogielska & Aldrich, 1999; Immke et al., 1999; Zhou et al., 2001) not only in K^+ channels, but also in Ca^{2+} channels (Dang & McClesky, 1998). Already Demo and Yellen (1992) said "that the effect of permeant ions on gating occurs through their interaction with binding sites within the pore". Such bindings sites are discussed by many authors (Matteson & Swenson, 1986; Demo & Yellen, 1992; Levy & Deutsch, 1996). Lu et al. (2001) realized that there is an interaction of Tl^+ with the selectivity filter in accordance with the findings of Choe et al. (2000) that K^+ ions can trigger conformational changes of the selectivity filter of Kir1.1b. A binding site in the pore itself would be in line with our finding that the AMFE occurs when the current drags Tl^+ into the pore.

Deep energetic valleys as suggested by the Hille-Schwarz model (1978) do not exist (Bernéche & Roux, 2001). Instead, conformational changes induced by the ions in the selectivity filter have to be considered. Even if a negative charge adjacent to the GYG motif (D378T in Kv2.1: Kirsch et al., 1995) is mutated, the effect of ionic strength indicates that it is not electrostatic interaction that causes the observed changes in Na^+/K^+ selectivity and gating (but an effect on conformational changes). In light of these results, probably the suggestions of Lu et al. (2001) on the role of thiolate groups of C169 for generating the AMFE have to be modified. The authors assumed

that C169 pointing directly at the cavity can trap one Tl^+, but this residue may also be involved in stabilizing the P-loop, like A463C in the studies of Ogielska and Aldrich (1999).

The Role of Models 1 and 2

Even though the concentration dependence of temporal behavior has ruled out models 1 and 2, they still may play a role in further studies. The left-hand part of Fig. 7 is a Markov model of the occupation of the locations 1, 2, 3, 4 in the pore similar to the model in Fig. 4 of Morais-Cabral et al. (2001). However, the number of four is not crucial. Many of the conclusions can be transferred to a model with two sites. In such a future role of models 1 and 2, the immediate output is not single-channel current but, as mediated by the integrating unit in the middle of Fig. 7, it adjusts the values of rate constants. However, as the ratio of open to closed times determines the apparent (averaged) single-channel current, the action of ion binding on this current may become very similar to that shown in Figs. 2 and 4.

The Role of Temporal Resolution in Measuring Apparent Single-Channel Currents

When the effect of the filters of the experimental setup on the measured (apparent) single-channel current was considered, Hansen et al. (1997) had the opinion that over a wide range of temporal resolutions the measured current would change gradually. This view was initiated by the Cs^+ block in *Chara* (Draber & Hansen, 1994). The full open-channel current (not observable at 5 kHz) was reached with 100-kHz sampling rate without any tricks as required in the approach employed for the AMFE (Farokhi et al., 2000). Further, Blunck found that lowering temperature made the apparent single-channel currents in the presence of 125 mM Na^+ and those in pure K^+ merge at 7°C along continuous lines (Hansen et al., 1997).

A different understanding arises from Fig. 3. With adequate rate constants $k_{1,1}$ and $k_{-1,S}$, the probability of state KKKK in pure K^+ solution is close to 1. Consequently, the related real single-channel current is correctly measured at all sampling rates. The probability of being open is decreased in the range of the AMFE (Figs. 1 and 2) to about 75%. Thus, also the gating-mediated current reduction of the AMFE is found to be equal for all temporal resolutions employed so far, and this explains the observation that the same current reduction was obtained with filters ranging from 1 kHz to 50 kHz.

Conclusion

Further research will modify some of the above assumptions of a gating-mediated AMFE. However, the basic message remains that gating models of the AMFE are feasible and that they can replace the permeation models like those of Hille & Schwarz (1978). Wu (1991, 1992) or others (Nonner, Chen & Eisenberg, 1998).

This work was supported by the Deutsche Forschungsgemeinschaft. We are grateful to Indra Schröder for critical reading.

References

Albertsen, A., Hansen, U.P. 1994. Estimation of kinetic rate constants from multi-channel recordings by a direct fit of the time series. *Biophys. J.* **67:**1393–1403

Antonov, S.M., Johnson, J.W. 1999. Permeant ion regulation of *N*-methyl-D-aspartate receptor channel block by Mg^{2+}. *Proc. Natl. Acad. Sci. USA* **96:**14571–14576

Balasubramanian, S., Lynch, J.W., Barry, P.H. 1997. Concentration dependence of sodium permeation and sodium ion interactions in the cyclic AMP-gated channels of mammalian olfactory receptor neurons. *J. Membrane Biol.* **159:**41–52

Ball, F.G., Rice, J.A. 1992. Stochastic models for ion channels: introduction and bibliography. *Math. Biosci.* **112:**189–206

Baukrowitz, T., Yellen, G. 1996. Use-dependent blockers and exit rate of the last ion from a multi-ion pore of a K^+ channel. *Science* **271:**653–656

Berněche, S., Roux, B. 2001. Energetics of ion conduction through the K^+ channel. *Nature* **414:**73–76

Blatt, M.R. 1988. Potassium-dependent bipolar gating of potassium channels in guard cells. *J. Membrane Biol.* **102:**235–246

Blunck, R., Kirst, U., Rießner, T., Hansen, U.P. 1998. How powerful is the dwell-time analysis of multi-channel records? *J. Membrane Biol.* **165:**19–35

Caliebe, A., Rösler, U., Hansen, U.P. 2002. A χ^2 test for model determination and sublevel detection in ion channel analysis. *J. Membrane Biol.* **185:** 25–41

Chapman, L., VanDongen, H.M., VanDongen, A.M. 1997. Activation-dependent subconductance levels in the drk1 channel suggest a subunit basis for ion permeation and gating. *Biophys. J.* **72:**702

Chen, T.Y., Miller, C. 1996. Nonequilibrium gating and voltage dependence of the ClC-O Cl^- channel. *J. Gen. Physiol.* **108:**237–250

Choe, H., Sackin, H., Palmer, L.G. 2000. Permeation properties of inward-rectifier potassium channels and their molecular determinants. *J. Gen. Physiol.* **115:**391–404

Ciani, S., Krasne, S., Miyazaki, S., Hagiwara, S. 1978. A model for anomalous rectification: electrochemical-potential-dependent gating of membrane channels. *J. Membrane Biol.* **44:**103–134

Colquhoun, D., Hawkes, A.G., Srodzinski, K. 1996. Joint distributions of apparent open times and shut times of single ion channels and the maximum likelihood fitting of mechanisms. *Phil. Trans. R. Soc. Lond. A* **354:**2555–2590

Dang, T.X., McClesky, E.W. 1998. Ion channel selectivity through stepwise changes in binding affinity. *J. Gen. Physiol.* **111:**185–193

Demo, S.D., Yellen, G. 1992. Ion effects of gating of the Ca^{2+} activated K^+ channel correlate with occupancy of the pore. *Biophys. J.* **61:**639–648

Dietrich, P., Hedrich, R. 1998. Anions permeate and gate GCAC1, a voltage-dependent guard cell anion channel. *Plant J.* **15:**479–487

Doyle, D.A., Cabral, J.M., Pfuetzner, R.A., Kuo, A., Gulbis, J.M., Cohen, S.L., Chait, B.T., MacKinnon, R. 1998. The structure

of the potassium channel: molecular basis of K^+ conduction and selectivity. *Science* **280:**69–77

Draber, S., Hansen, U.P. 1994. Fast single-channel measurements resolve the blocking effect of Cs^+ on the K^+ channel. *Biophys. J.* **67:**120–129

Draber, S., Schultze, R. 1994. Correction for missed events based on a realistic model of a detector. *Biophys. J.* **66:**191–201

Draber, S., Schultze, R., Hansen, U.P. 1991. Patch-clamp studies on the anomalous mole fraction effect of the K^+ channel in cytoplasmic droplets of *Nitella:* an attempt to distinguish between a multi-ion single-file pore and an enzyme kinetic model with lazy state. *J. Membrane Biol.* **123:**183–190

Eisenman, G., Latorre, R., Miller, C. 1986. Multi-ion conduction and selectivity in the high-conductance Ca^{2+}-activated K^+ channel from skeletal muscle. *Biophys. J.* **50:**1025–1034

Elber, R., Karplus, M. 1987. Multiple conformational states of proteins: a molecular dynamics analysis of myoglobin. *Science* **235:**318–321

Farokhi, A., Keunecke, M., Hansen, U.P. 2000. The Anomalous Mole Fraction Effect in *Chara*: gating at the edge of temporal resolution. *Biophys. J.* **79:**3072–3082

Feng, Z.-P., Hamid, J., Doering, C., Jarvis, S.E., Bosey, G.M., Bourinet, E., Snutch, T.P., Zamponi, G.W. 2001. Amino acid residues outside of the pore region contribute to N-type calcium channel permeation. *J. Biol. Chem.* **276:**5726–5730

Ferguson, W.B., McManus, O.B., Magleby, K.L. 1993. Opening and closing transitions for BK channels often occur in two steps via sojourns through a brief lifetime subconductance state. *Biophys. J.* **65:**702–714

Fredkin, D.R., Rice, J.A. 1992. Maximum likelihood estimation and identification directly from single-channel recordings. *Proc. Roy. Soc. Land.* **B 249:**125–132

Friel, D.D., Tsien, R.W. 1989. Voltage-gated calcium channels: direct observation of the anomalous mole fraction effect at the single channel level. *Proc. Natl. Acad. Sci. USA* **86:**5207–5211

Hagiwara, S., Miyazaki, S., Krasne, S., Ciani, S. 1977. Anomalous permeabilities of the egg cell membrane of a starfish in K^+/Tl^+ mixtures. *J. Gen. Physiol.* **70:**269–281

Hansen, U.P. (1986). Reaction kinetic models of pumps, cotransporters and channels. *In:* Ion Channels and Electrogenic Pumps in Biomembranes. Abstracts of Lectures and Posters. U. Kishimoto, editor pp. L13–L33. Osaka University, Japan

Hansen, U.P., Gradmann, D., Sanders, P., Slayman, C.L. 1981. Interpretation of current-voltage relationships for "active" ion transport systems: I. Steady-state reaction-kinetic analysis of Class-I mechanisms. *J. Membrane Biol.* **63:**165–190

Hansen, U.P., Keunecke, M., Blunck, R. 1997. Gating and permeation models of plant channels. *J. Exp. Bot.* **48:**365–382

Hansen, U.P., Tittor, J., Gradmann, D. 1983. Interpretation of current-voltage relationships for "active" ion transport systems: II. Nonsteady-state reaction kinetic analysis of class I mechanisms with one slow time constant. *J. Membrane Biol.* **75:**141–169

Hess, P., Tsien, R.W. 1984. Mechanism of ion permeation through calcium channels. *Nature* **309:**453–456

Hille, B., Schwarz, W. 1978. Potassium channels as multi-ion single-file pores. *J. Gen. Physiol.* **72:**409–442

Immke, D., Wood, M., Kiss, L., Korn, S.J. 1999. Potassium-dependent changes in the conformation of the Kv2.1 potassium channel pore. *J. Gen. Physiol.* **113:**819–836

Jackson, M.B. 1997. Inversion of Markov processes to determine rate constants from single-channel data. *Biophys. J.* **73:**1382–1394

Junge, W., Lill, H., Engelbrecht, S. 1997. ATP synthase: an electrochemical transducer with rotatory mechanics. *Trends Biochem. Sci.* **22:**420–423

Kiss, L., Korn, S.J. 1998. Modulation of C-type inactivation by K^+ at the potassium channel selectivity filter. *Biophys. J.* **74:**1840–1849

Kiss, L., Immke, D., Turco, J.L., Korn, S. 1998. The interaction of Na^+ and K^+ in voltage-gated potassium channels. Evidence for cation binding sites of different activity. *J. Gen. Physiol.* **111:**195–206

Kiss, T., LoTurco, J., Korn, S.J. 1999. Contribution of the selectivity filter to inactivation in potassium channels. *Biophys. J.* **76:**253–263

Kirsch, G.E., Pascual, J.M., Sheih, C.-C. 1995. Functional role of a conserved aspartate in the external mouth of voltage-gated potassium channels. *Biophys. J.* **68:**1804–1813

Klein, S., Timmer, J., Honerkamp, J. 1997. Analysis of multi channel patch clamp recordings by Hidden Markov models. *Biometrics* **53:**870–884

Klieber, H.G., Gradmann, D. 1993. Enzyme kinetics of the prime K^+ channel in the tonoplast of *Chara*: selectivity and inhibition. *J. Membrane Biol.* **132:**253–265

Korn, S.J., Horn, R. 1988. Statistical discrimination of fractal and Markov models of single-channel gating. *Biophys. J.* **54:**871–877

Larsson, H.P., Elinder, F. 2000. A conserved glutamate is important for slow inactivation in K^+ channels. *Neuron* **27:**573–583

Levy, D.I., Deutsch, C. 1996. Recovery from C-type inactivation is modulated by extracellular potassium. *Biophys. J.* **70:**798–805

Loots, E., Isacoff, E.Y. 2000. Molecular coupling of S4 to a K^+ channel's slow inactivation gate. *J. Gen. Physiol.* **116:**623–635

Lu, T., Wu, L., Xiao, J., Yang, J. 2001. Permeant ion-dependent changes in gating of Kir2.1 inward rectifier potassium channels. *J. Gen. Physiol.* **118:**509–521

Lühring, H.E. 1986. Recording of single channel K^+ channels in the membrane of cytoplasmic drop of *Chara australis*. *Protoplasma* **133:**19–28.

Luhring, H.E. 1999. pH-sensitive gating kinetics of the Maxi-K channel in the tonoplast of *Chara australis*. *J. Membrane Biol.* **168:**47–61

Magleby, K.L. 2001. Commentary: Kinetic gating mechanisms for BK channels: when complexity leads to simplicity. *J. Gen. Physiol.* **118:**583–587

Mathur, R., Zheng, J., Yan, Y., Sigworth, F.J. 1997. Role of the S3-S4 linker in *Shaker* potassium channel activation. *J. Gen. Physiol.* **109:**191–199

Matteson, D.R., Swenson, R.P. 1986. External monovalent cations that impede the closing by acting at a site in the channel. *J. Gen. Physiol.* **87:**795–816

Melishchuk, A., Loboda, A., Armstrong, C.M. 1998. Loss of *Shaker* K channel conductance in 0 K^+ solutions: role of the voltage sensor. *Biophys. J.* **75:**1828–1835

Morais-Cabral, J.H., Zhou, Y., MacKinnon, R. 2001. Energetic optimization of ion conduction rate by the K^+ selectivity filter. *Nature* **414:**37–42

Moss, B.L., Magleby, K.L. 2001. Gating and conductance properties of BK channels are modulated by the S9-S10 tail domain of the α subunit. A study of mSlo1 and mSlo3 wild-type and chimeric channels. *J. Gen. Physiol.* **118:**711–734

Nonner, W., Chen, D.P., Eisenberg, B. 1998. Anomalous mole fraction effect, electrostatics, and binding in ionic channels. *Biophys. J.* **74:**2327–2334

Ogielska, E.M., Aldrich, R.W. 1999. Functional consequences of a decreased potassium affinity in a potassium channel pore: ion interaction and C-type inactivation. *J. Gen. Physiol.* **113:**347–358

Pardo, L.A., Heinemann, S.H., Terlau, H., Ludewig, C., Lorra, O., Pongs, O., Stühmer, W. 1992. Extracellular K^+ specifically

modulates a rat brain K^+ channel. *Proc. Natl. Acad. Sci. USA* **89:**2466–2470

Perozo, E., Cortes, D.M., Cuello, L.G. 1999. Structural rearrangements underlying K^+ channel activation gating. *Science* **285:**73–78

Pietrobon, D., Prod'hom, B., Hess, P. 1988. Conformational changes associated with ion permeation in L-type calcium channels. *Nature* **333:**373–376

Proks, P., Capener, C.E., Jones, P., Ashcroft, F.M. 2001. Mutations within the P-loop of Kir6.2 modulate the intraburst kinetics of the ATP-sensitive potassium channel. *J. Gen. Physiol.* **118:**341–353

Pusch, M. 1996. Knocking at the channel's door. The permeating chloride ion acts as the gating charge in ClC-O. *J. Gen. Physiol.* **108:**233–236

Pusch, M., Ludewig, U., Rehfeldt, A., Jentsch, T.J. 1995. Gating of the voltage-dependent chloride channel ClC-O by the permeant anion. *Nature* **373:**527–531

Riessner, T., Woelk, F., Abshagen, M., Hansen, U.P. 2002. A new level detector for ion channel analysis. *J. Membrane Biol.* **189:**105–118

Rosenmund, C., Stern-Bach, Y., Stevens, C.F. 1998. The tetrameric structure of a glutamate receptor channel. *Science* **280:**1596–1599

Rothberg, B.S., Magleby, K.L. 2000. Voltage and Ca^{2+} activation of single large-conductance Ca^{2+}-activated K^+ channels described by a two-tiered allosteric gating mechanism. *J. Gen. Physiol.* **116:**75–99

Ruiz, M.L., Karpen, J.W. 1999. Opening mechanism of a cyclic nucleotide-gated channel based on analysis of single channels locked in each liganded state. *J. Gen. Physiol.* **113:**873–895

Sakano, K., Tazawa, M. 1986. Tonoplast origin of the envelope membrane of cytoplasmic droplets prepared from *Chara* internodal cells. *Protoplasma* **131:**247–249

Sanders, D., Hansen, U.P. 1981. Mechanism of Cl^- transport at the plasma membrane of *Chara corallina*. II. Transinhibition and the determination of H^+/Cl^- binding order from a reaction kinetic model. *J. Membrane Biol.* **58:**139–153

Schneggenburger, R., Ascher, P. 1997. Coupling of permeation and gating in an NMDA-channel pore mutant. *Neuron* **18:**167–177

Schultze, R., Draber, S. 1993. A nonlinear filter algorithm for detection of jumps in patch-clamp data. *J. Membrane Biol.* **132:**41–52

Shi, J., Cui, J. 2001. Intracellular Mg^{2+} enhances the function of BK-type Ca^{2+}-activated K^+ channel. *J. Gen. Physiol.* **118:**589–605

Sunderman, E.R., Zagotta, W.N. 1999a. Mechanism of allosteric modulation of rod cyclic nucleotide gated channels. *J. Gen. Physiol.* **113:**601–620

Sunderman, E.R., Zagotta, W.N. 1999b. Sequence of events underlying the allosteric transition of rod cyclic nucleotide gated channels. *J. Gen. Physiol.* **113:**621–640

Swenson, R.P., Armstrong, C.M. 1981. K^+ channels close more slowly in the presence of external K^+ and Rb^+. *Nature* **291:**427–429

Tabcharani, J.A., Rommens, J.M., Hou, Y.X., Chang, X.B., Tsui, L.C., Riordan, J.R., Hanrahan, J.W. 1993. Multi-ion pore behavior in the CFTR chloride channel. *Nature* **366:**79–82

Tester, M. 1988. Potassium channels in the plasmalemma of *Chara corallina* are multi-ion pores: voltage-dependent blockade by Cs^+ and anomalous permeabilities. *J. Membrane Biol.* **105:**87–94

Townsend, C., Horn, R. 1999. Interaction between the pore and the fast gate of the cardiac sodium channel. *J. Gen. Physiol.* **113:**321–331

Wagoner, P.K., Oxford, G.S. 1987. Cation permeation through the voltage-dependent potassium channel in the squid axon. *J. Gen. Physiol.* **90:**261–290

Wood, M.J., Korn, S.J. 2000. Two mechanisms of K^+-dependent potentiation in Kv2.1 potassium channels. *Biophys. J.* **79:**2335–2546

Wu, J. 1991. Microscopic model for selective permeation in ion channels. *Biophys. J.* **60:**238–251

Wu, J. 1992. Dynamic ion-ion and water-ion interactions in ion channels. *Biophys. J.* **61:**1316–1331

Yellen, G., Sodickson, D., Chen, T.-Y., Jurman, M.E. 1994. An engineered cysteine in the external mouth of a K^+ channel allows inactivation to be modulated by metal binding. *Biophys. J.* **66:**1068–1075

Yeo, G.F., Milne, R.K., Edeson, R.O., Madsen, B.W. 1988. Stastistical inference from single channel records: two-state Markov model with limited time resolution. *Proc. R. Soc. Lond.* **B 235:**63–94

Yool. A.J., Schwarz, T.L. 1996. Anomalous mole fraction effect induced by mutation of the H5 pore region in the K^+ *Shaker* channel. *Biophys. J.* **71:**2467–2472

Zhang, X., Solaro, C.R., Lingle, C.J. 2001. Allosteric regulation of BK channel gating by Ca^{2+} and Mg^{2+} through a non-selective, low affinity divalent cation site. *J. Gen. Physiol.* **118:**607–635

Zheng, J., Sigworth, F.J. 1997. Selectivity changes during activation of mutant Shaker potassium channels. *J. Gen. Physiol.* **110:**101–117

Zheng, J., Vankataramanan, L., Sigworth, F.J. 2001. Hidden Markov model analysis of intermediate gating steps associated with the pore gate of Shaker potassium channels. *J. Gen. Physiol.* **118:**547–562

Zhou, Y., Morais-Cabral, J.H., Kaufman, A., MacKinnon, R. 2001. Chemistry of ion coordination and hydration revealed by a K^+ channel-Fab complex at 2.0 Å resolution. *Nature* **414:**42–48